Voyager Interstellar

John Belcher
617-253-4285
37-695 MIT
77 Massachusetts Avenue
Cambridge MA 02139

A pdf copy of this word document not too far out of date can be found at
http://web.mit.edu/jbelcher/www/VoyagerInterstellar.pdf
and the word document itself is at
http://web.mit.edu/jbelcher/www/VoyagerInsterstellar.doc

Comments and questions to jbelcher@mit.edu

Contents

1 Overview

1.1 Important Dates

The launch dates of the Voyager I and II spacecraft were September 5 (DOY 248, first M mode spectrum at 1977 248 14) and August 20 (DOY 232, first M mode spectrum is at 1977 232 16 0 5 403), 1977, respectively. We discuss the PLS experiment's location on the spacecraft and its measurement capabilities.

Voyager 1:

Event	Date
1st M mode spectrum after launch	1977 248 1400
1st Inbound Jovian Bow Shock	1979 59 1434
Final PLS failure	1980 328 1024
Heliopause	8/25/2012

Voyager 2:

Event	Date
1st M mode spectrum after launch	1977 232 1605
1st Inbound Jovian Bow Shock	1979 183 1619
Final PLS failure	1980 328 1024
Heliopause	8/25/2012

The launch vehicle is pictured below, see http://historicspacecraft.com/Archives.html

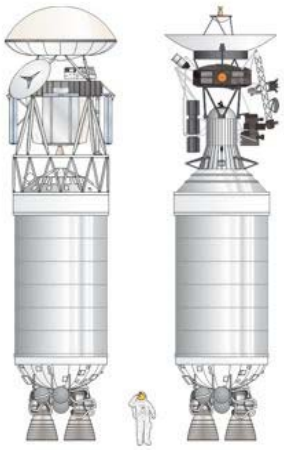

2 Spacecraft and PLS Instrument

2.1 Configuration

The Plasma Science Experiment (PLS) is shown below. The various cups in the main sensor (A, B, C) have normals which make an angle of 20 degrees to the symmetry axis of the main sensor.

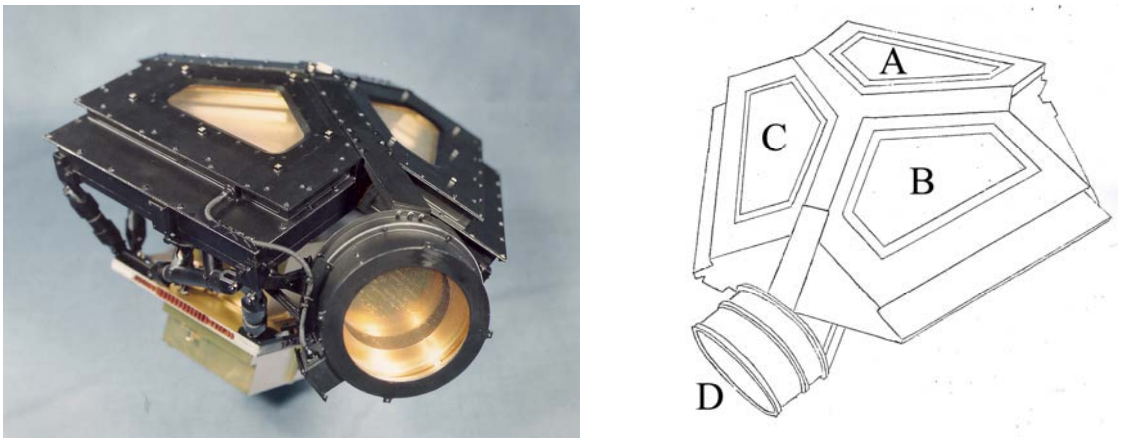

Figure 2.1-1: The Four Sensors of the Plasma Science Experiment

The experiment is mounted on the science boom as shown in the figures below.

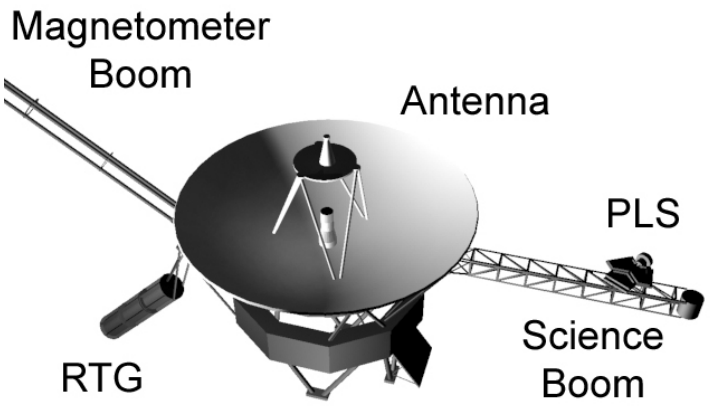

Figure 2.1-2: The Voyager Spacecraft

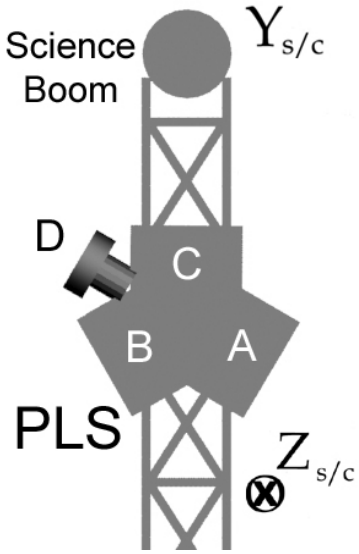

Figure 2.1-3: Close up of Science Boom and PLS Instrument

2.2 Spacecraft Coordinates and Cup Normals

The symmetry axis of the main PLS cluster is along the negative spacecraft Z axis (see Figure 2.2.1), which is aligned with spacecraft antenna. Thus when the spacecraft antenna is pointed at the earth (the usual configuration), the negative spacecraft Z axis points toward the earth, as does the symmetry axis of the main cluster. The definition of the spacecraft axes are shown in Figure 2.2.1.

The various cup normals to the four plasma sensors in spacecraft coordinates are given by

$$\hat{\mathbf{n}}_A = -\hat{\mathbf{X}}_{s/c} \sin 20^o \cos 30^o - \hat{\mathbf{Y}}_{s/c} \sin 20^o \cos 60^o - \hat{\mathbf{Z}}_{s/c} \cos 20^o \tag{2.2.1}$$

$$\hat{\mathbf{n}}_B = \hat{\mathbf{X}}_{s/c} \sin 20^o \cos 30^o - \hat{\mathbf{Y}}_{s/c} \sin 20^o \cos 60^o - \hat{\mathbf{Z}}_{s/c} \cos 20^o \tag{2.2.2}$$

$$\hat{\mathbf{n}}_C = \hat{\mathbf{Y}}_{s/c}\sin 20^\circ - \hat{\mathbf{Z}}_{s/c}\cos 20^\circ \tag{2.2.3}$$

$$\hat{\mathbf{n}}_D = \hat{\mathbf{X}}_{s/c}\cos 43^\circ + \hat{\mathbf{Y}}_{s/c}\sin 43^\circ \tag{2.2.4}$$

We can invert this non-orthogonal transformation to obtain

$$\hat{\mathbf{X}}_{s/c} = \frac{\hat{\mathbf{n}}_B - \hat{\mathbf{n}}_A}{2\sin 20\cos 30} \tag{2.2.5}$$

$$\hat{\mathbf{Y}}_{s/c} = \frac{1}{\sin 20^\circ\left(1+\cos 60^\circ\right)}\left[\hat{\mathbf{n}}_C - \frac{\hat{\mathbf{n}}_A + \hat{\mathbf{n}}_B}{2}\right] \tag{2.2.6}$$

$$\hat{\mathbf{Z}}_{s/c} = -\left[\frac{\hat{\mathbf{n}}_A + \hat{\mathbf{n}}_B}{2\cos 60^\circ} + \hat{\mathbf{n}}_C\right]\left[\frac{\cos 60^\circ}{\cos 20^\circ\left(1+\cos 60^\circ\right)}\right] \tag{2.2.7}$$

When in the supersonic solar wind, the various cups in the main sensor measure the components of proton velocity *along the direction anti-parallel to the sensor normal*, so if V_A, V_B, and V_C are the measured components of the solar wind speed along the cup normals, they are related to the solar wind components in spacecraft coordinates by

$$V_A = V_{X\,s/c}\sin 20^\circ\cos 30^\circ + V_{Y\,s/c}\sin 20^\circ\cos 60^\circ + V_{Z\,s/c}\cos 20^\circ \tag{2.2.8}$$

$$V_B = -V_{X\,s/c}\sin 20^\circ\cos 30^\circ + V_{Y\,s/c}\sin 20^\circ\cos 60^\circ + V_{Z\,s/c}\cos 20^\circ \tag{2.2.9}$$

$$V_C = -V_{Y\,s/c}\sin 20^\circ + V_{Z\,s/c}\cos 20^\circ \tag{2.2.10}$$

and conversely

$$V_X = \frac{V_A - V_B}{2\sin 20\cos 30} \tag{2.2.11}$$

$$V_Y = \frac{1}{\sin 20^\circ\left(1+\cos 60^\circ\right)}\left[-V_C + \frac{V_A + V_B}{2}\right] \tag{2.2.12}$$

$$V_Z = \left[\frac{\cos 60^\circ}{\cos 20^\circ\left(1+\cos 60^\circ\right)}\right]\left[\frac{V_A + V_B}{2\cos 60^\circ} + V_C\right] \tag{2.2.13}$$

Numerically, we have for the cup normals the following values

	Xs/c	Ys/c	Zs/c
A cup	-0.296198	-0.171010	-0.939693
B cup	0.296198	-0.171010	-0.939693
C cup	0.000000	0.342020	-0.939693
D cup	0.731354	0.681998	0.000000

(2.2.14)

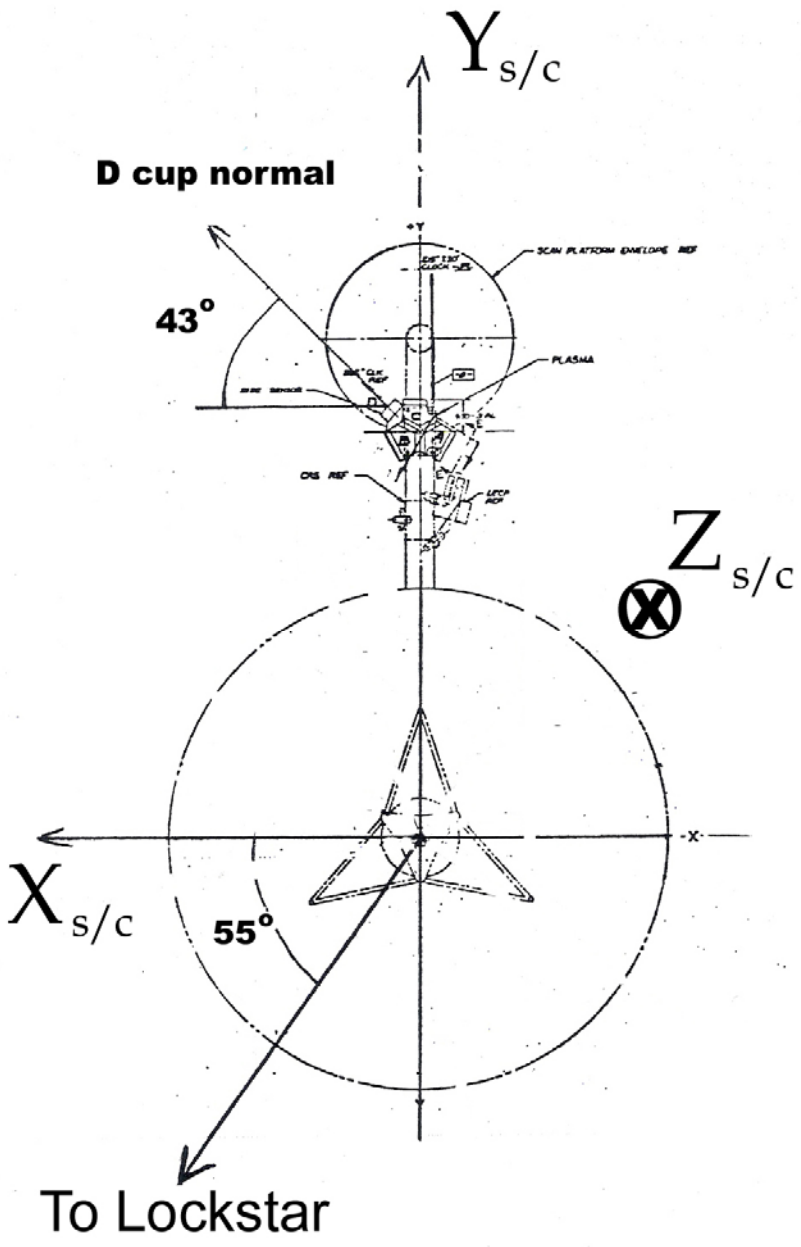

Figure 2.2-4: Spacecraft Coordinates

2.3 The Canopus Sensor

Consider a spherical polar coordinate system based on spacecraft coordinates. The Canopus sensor is an slit which is narrow in azimuth in this system. The narrow azimuth extent of the slit is centered at -55 degrees in azimuth (see Figure above). The slit is elongated in the polar angle, with the center of the elongated slit at a polar angle of 90 degrees (that is, in the $X_{s/c}$-$Y_{s/c}$ plane). When the Canopus sensor is on a given lock star, the direction to that star will lie somewhere in a plane perpendicular to the $X_{s/c}$-$Y_{s/c}$ plane with an azimuth angle of -55 degrees.

3 Instrument

3.1 Introduction

The Voyager I instrument failed just past Saturn encounter. The Voyager II instrument continues to operate up to the present time. A full description of the instrument is given in Bridge et al. (1977).

3.2 The Experimental Concept

The Voyager measurement concept for a supersonic plasma such as the solar wind provides: (1) complete coverage of phase space with high time resolution; (2) determination of the density, velocity, pressure tensor, and heat flux, with no model : The assumptions; (3) ease of data interpretation—that is the above properties can be obtained by the formation of sums based directly on the measured currents; (4) ease of a non-linear least squares fit analysis if desired.

These features are achieved the use of a cluster of three modulated grid Faraday cup plasma detectors (Figure 2.2-1). The axis of symmetry of the cluster (the spacecraft $-\hat{\mathbf{z}}$ direction) is approximately along the spacecraft-earth line, which is close to the spacecraft-sun line. The normal to each of the three cups (referred to as the A, B, and C detectors) are each 20 degrees from the symmetry axis and 120 degrees apart in azimuth. Each detector has an extremely wide field of view for full acceptance of the incident plasma ions, and the cluster as a whole has a common field of view which is a cone of approximately 45 degrees half-angle about the symmetry axis. All detectors have full acceptance in this common field of view.

3.2.1 Voltage Levels

Let Φ_k be the lower modulator voltage for the k-th energy window (*k* runs from 1 to 16 for the *L* (low resolution) ion mode and from 1 to 128 for the *M* (high resolution) ion mode. Then for the *L* mode, these lower (upper) voltage in channel k (k-1) are given by

$$\Phi_k = \left[60\left(1.33352\right)^{k-1} - 50 \right] \text{ Volts} \quad k = 1 \text{ to } 17 \tag{3.2.1.1}$$

and in the *M* mode by

$$\Phi_k = \left[60\left(1.03663\right)^{k-1} - 50 \right] \text{ Volts} \quad k = 1 \text{ to } 129 \tag{3.2.1.2}$$

Table 3-1 shows the various voltages and speeds in the *L* mode.

channel	Lower voltage	Lower speed	Average Speed	Delta Speed
1	10.0	43.8	59.8	32.1
2	30.0	75.8	90.0	28.4
3	56.7	104.2	118.6	28.7
4	92.3	133.0	148.3	30.7
5	139.7	163.6	180.4	33.6
6	203.0	197.2	215.9	37.4
7	287.4	234.7	255.7	42.2
8	399.9	276.8	300.7	47.8
9	550.0	324.6	351.9	54.5
10	750.1	379.1	410.3	62.3
11	1017.0	441.4	477.1	71.4
12	1372.8	512.9	553.9	82.1
13	1847.3	594.9	642.1	94.4
14	2480.1	689.3	743.7	108.7
15	3324.0	798.0	860.7	125.3
16	4449.3	923.3	995.5	144.4
17	5949.9	1067.7		

Table 3-1: Voltages and speeds for the L mode

In Table 1, a given voltage Φ_k corresponds to a proton speed given by

$$\tfrac{1}{2} m_{proton} \mathrm{v}_k^2 = q_{proton} \Phi_k \quad \text{or} \quad \mathrm{v}_k = \sqrt{\frac{2 q_{proton} \Phi_k}{m_{proton}}} = 13841.8 \sqrt{\Phi_k} \tag{3.2.1.3}$$

where in the last equation, if Φ_k is given in volts, then the speed is in km/s.

3.2.2 Reduced Distribution Function and Measured Currents

To understand the Voyager moments calculation, let $\hat{\mathbf{n}}$ be the unit normal to a given collector, and $\hat{\mathbf{t}}_1$ and $\hat{\mathbf{t}}_2$ be mutually perpendicular unit vectors which are transverse to $\hat{\mathbf{n}}$. Let A be the area of the sensor, and q_{proton} the charge on a proton. If v_k is the lower speed for the k-th energy channel, then the modulated current I_k measured by the Faraday cup for the k-th channel is related to the particle distribution function $f(\mathbf{v})$ by:

$$I_k = q_{proton} A \int_{\mathrm{v}_k}^{\mathrm{v}_{k+1}} d\mathrm{v}_n \mathrm{v}_n \int_{-\infty}^{\infty} \int_{-\infty}^{\infty} d\mathrm{v}_{t1} d\mathrm{v}_{t2} f(\mathbf{v}) G(\mathbf{v}, \hat{\mathbf{n}}) \tag{3.2.2.1}$$

In this expression $f(\mathbf{v})$ is the distribution function, $G(\mathbf{v}, \hat{\mathbf{n}})$ is the fraction of the aperture that intercepts the collector when projected in a given direction $\mathbf{v}$, and (v_n, v_{t1}, v_{t2}) are the components of the velocity along ($\hat{\mathbf{n}}, \hat{\mathbf{t}}_1, \hat{\mathbf{t}}_2$). The three cups in the main cluster have

been carefully designed to have wide fields of view, so that in the solar wind, the function $G(\mathbf{v},\hat{\mathbf{n}})$ in equation (3.2.2.1) can be taken to be simply the transparency of the grids for all reasonable angles of incidence of the solar wind.

In addition in the inner solar system the thermal speed of the protons is much greater than the width of the channels in speed, as the velocity windows are narrow ($\Delta v / v \approx 1.8\%$), so that in equation (3.2.2.1) it is reasonable to assume that the distribution function is only slowly varying over a channel. With this assumption, and defining the average and difference speeds for a given channel as

$$\overline{v}_k = (v_{k+1}+v_k)/2 \qquad\qquad \Delta v_k = (v_{k+1}-v_k) \tag{3.2.2.2}$$

we can write equation (3.2.2.1) as

$$I_k = q_{proton} A_{eff} \Delta v_k \overline{v}_k \int_{-\infty}^{\infty}\int_{-\infty}^{\infty} dv_{t1} dv_{t2}\, f\left(\overline{v}_k, v_{t1}, v_{t2}\right) \tag{3.2.2.3}$$

where A_{eff} is the product of the area of the cups and the transparency of the grids. Let us define the reduced distribution function F as

$$F(v_n) = \int_{-\infty}^{\infty}\int_{-\infty}^{\infty} dv_{t1} dv_{t2}\, f\left(v_n, v_{t1}, v_{t2}\right) \tag{3.2.2.4}$$

From the above equations, it is clear that a good estimate of F evaluated at $\overline{v}_k$ is

$$F(v_n)\big|_{v_n=\overline{v}_k} = I_k / \left[q_{proton} A_{eff} \Delta v_k \overline{v}_k \right] \tag{3.2.2.5}$$

3.2.3 Moments Calculation

The direct connection between the measured currents and the reduced distribution function shown in equation (3.2.2.5) is the key to the simplicity of the Voyager data analysis in the warm, supersonic solar wind. Each detector samples the full distribution function in a manner which is differential for the velocity component parallel to the detector normal and integral for the velocity components perpendicular to the detector normal. The cluster as a whole provides measurements of the reduced distribution function in each of three well separated directions. This information can be used to obtain the moments of the full distribution function *f*, given the magnetic field direction, in a straight forward manner, as follows.

The definition of the moments of *f* through the third moment are given by

$$N = \iiint f\, d^3v \tag{3.2.3.1}$$

$$\mathbf{V} = \iiint \mathbf{v}\, f\, d^3\mathrm{v} / N \tag{3.2.3.2}$$

$$\vec{\mathbf{P}} = m\iiint (\mathbf{v}-\mathbf{V})(\mathbf{v}-\mathbf{V})\, f\, d^3\mathrm{v} \tag{3.2.3.3}$$

$$\vec{\mathbf{Q}} = \tfrac{1}{2} m\iiint (\mathbf{v}-\mathbf{V})(\mathbf{v}-\mathbf{V})(\mathbf{v}-\mathbf{V})\, f\, d^3\mathrm{v} \tag{3.2.3.4}$$

where $\vec{\mathbf{P}}$ is a the second rank pressure tensor and $\vec{\mathbf{Q}}$ is the third rank heat flux tensor. If we assume that f is gyrotropic, then we can write

$$\vec{\mathbf{P}} = (P_{\parallel} - P_{\perp})\hat{\mathbf{b}}\hat{\mathbf{b}} + P_{\perp}\vec{\mathbf{I}} \tag{3.2.3.5}$$

$$\vec{\mathbf{Q}} = Q_{\parallel}\hat{\mathbf{b}}\hat{\mathbf{b}}\hat{\mathbf{b}} + Q_{\perp}\vec{\mathbf{I}}\hat{\mathbf{b}} \tag{3.2.3.6}$$

where $\hat{\mathbf{b}}$ is the unit vector along the magnetic field direction.

Consider a given detector with normal $\hat{\mathbf{n}}$. Let θ_n be the angle between the magnetic field direction and the cup normal. We can calculate the moments of F by approximating integrals by sums. From the equations above, it is clear that for each cup we can find the following moments of F.

$$N = \int F(\mathrm{v}_n)\, d\mathrm{v}_n = \sum_k \left[\frac{I_k}{q_{proton} A_{eff} \Delta\mathrm{v}_k \overline{\mathrm{v}}_k}\right] \Delta\mathrm{v}_k = \frac{1}{q_{proton} A_{eff}} \sum_k \left[\frac{I_k}{\overline{\mathrm{v}}_k}\right] \tag{3.2.3.7}$$

$$V_n = \int \mathrm{v}_n F(\mathrm{v}_n)\, d\mathrm{v}_n / N = \sum_k \overline{\mathrm{v}}_k \left[\frac{I_k}{q_{proton} A_{eff} \Delta\mathrm{v}_k \overline{\mathrm{v}}_k}\right] \Delta\mathrm{v}_k / N = \frac{1}{q_{proton} A_{eff}} \sum_k [I_k] / N \tag{3.2.3.8}$$

$$\begin{aligned} P_{nn} &= \hat{\mathbf{n}} \cdot \vec{\mathbf{P}} \cdot \hat{\mathbf{n}} = P_{\parallel} \cos^2\theta_n + P_{\perp} \sin^2\theta \\ &= m\int (\mathrm{v}_n - \mathrm{V}_n)^2 F(\mathrm{v}_n)\, d\mathrm{v}_n = \frac{m}{q_{proton} A_{eff}} \sum_k (\overline{\mathrm{v}}_k - \mathrm{V}_n)^2 \left[\frac{I_k}{\overline{\mathrm{v}}_k}\right] \end{aligned} \tag{3.2.3.9}$$

$$\begin{aligned} Q_{nnn} &= Q_{\parallel} \cos^3\theta_n + 3Q_{\perp} \cos\theta_n \\ &= \frac{m}{2}\int (\mathrm{v}_n - \mathrm{V}_n)^3 F(\mathrm{v}_n)\, d\mathrm{v}_n = \frac{m}{2q_{proton} A_{eff}} \sum_k (\overline{\mathrm{v}}_k - \mathrm{V}_n)^3 \left[\frac{I_k}{\overline{\mathrm{v}}_k}\right] \end{aligned} \tag{3.2.3.10}$$

Each of these equations is repeated for each of the three cups. Thus, knowledge of the field direction and the moments of the three reduced distribution functions is sufficient to determine N (three independent estimates), **V**, $P_{\parallel}$ and $P_{\perp}$ (over-determined), and $Q_{\parallel}$ and $Q_{\perp}$ (over-determined). The sums indicated in the equations above are carried out by the Fortran routine *moments.f* (see Section 5.4 below).

3.2.4 Relationship between Pressure, Temperature, and Thermal Speed

To calculate a thermal speed W_{nn}, we have the following relationships:

$$P_{nn} = NkT_{nn} = N\left[\tfrac{1}{2}mW_{nn}^2\right] \qquad W_{nn} = \sqrt{\frac{2P_{nn}}{mN}} \qquad T_{nn} = \frac{\tfrac{1}{2}mW_{nn}^2}{k} \qquad W_{nn} = \sqrt{\frac{2kT_{nn}}{m}} \qquad (3.2.4.1)$$

Comparing (3.2.4.1) with (3.2.3.9), we see that

$$W_{nn} = \sqrt{2\int \left(\mathrm{v}_n - \mathrm{V}_n\right)^2 F(\mathrm{v}_n)\, d\mathrm{v}_n / N} = \sqrt{\frac{2}{q_{proton}A_{eff}} \sum_k \left(\overline{\mathrm{v}}_k - \mathrm{V}_n\right)^2 \left[\frac{I_k}{\overline{\mathrm{v}}_k}\right] / N} \qquad (3.2.4.2)$$

3.2.5 Theoretical Examples of the Voyager Measurement Scheme

To illustrate this scheme with two concrete examples, we show in the two figures below two different samples of the same distribution function. The distribution function consists of two bi-Maxwellians, with one hotter than the other. In each case, the bottom panel of the figure shows iso-density contours of the distribution function. For ease of presentation, we have assumed that the bulk velocity **V**, the magnetic field **B**, and a given cup normal $\hat{\mathbf{n}}$ all lie in the plane of the paper.

Also indicated in the lower panel is the manner in which a given detector slices the distribution function for a given $\hat{\mathbf{n}}$. .In the upper panel we show the measured currents which would result from this sampling for a given $\hat{\mathbf{n}}$. Note in particular the difference between the measured currents in the case when $\hat{\mathbf{n}}$ has a large projection along **B** as contrasted to the case when $\hat{\mathbf{n}}$ has a small projection along **B**. Although over-idealized, these figures clearly illustrates in principle the three-dimensional capabilities of the Voyager measurements.

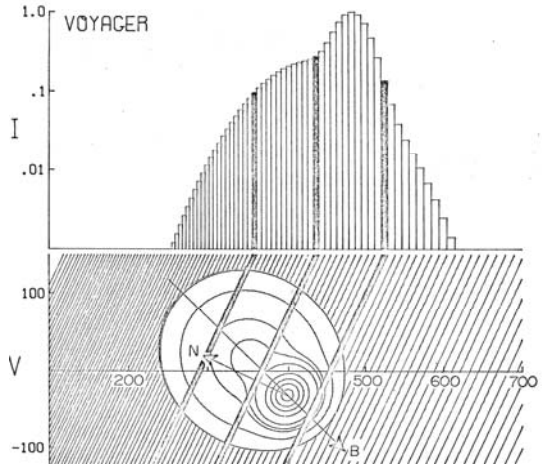

Figure 3.2-1: Theoretical currents, B and n close to parallel.

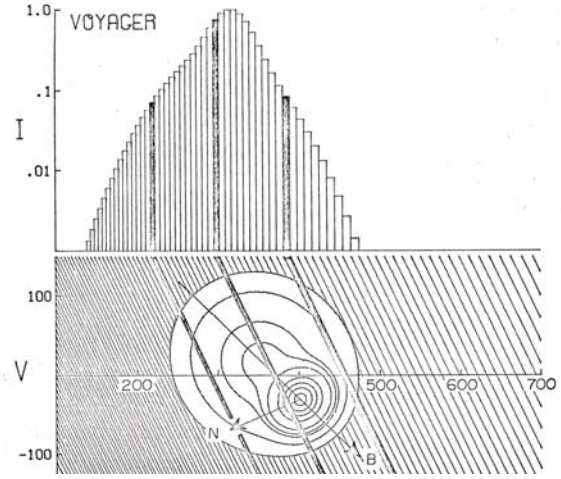

Figure 3.2-2: Theoretical currents, B and n close to perpendicular.

3.3 Measured Voyager Ion Spectra

3.3.1 Solar Wind M Modes

Figure 3.3-1 shows four sample spectra from the M mode sequence from early in the mission. Measured currents (fluxes) in each of the three detectors are indicated by the step-like lines. On each figure, we also give some of the results of the moment calcu1ations for the proton peak (see the discussion in II above and IV A below). In two of the figures, least squares fit points using Maxwellians are indicated by crosses and diamonds. The instrument quantizes the currents logarithmically using eight bits to cover a range of four decades for each gain state of the instrument. The quantization error is thus + 1.8%.The noise level is = 6 x 10^{-14} amps for the integration time used in the measurements presented here. At the highest bit rate, an M mode spectrum is obtained every twelve seconds. For the alpha particles particle distribution, the peak is located at

twice the energy of the proton peak in all detectors, because we are measuring energy per charge and an alpha particle moving at the same speed as a proton has twice the energy per charge (four times the mass and twice the charge).

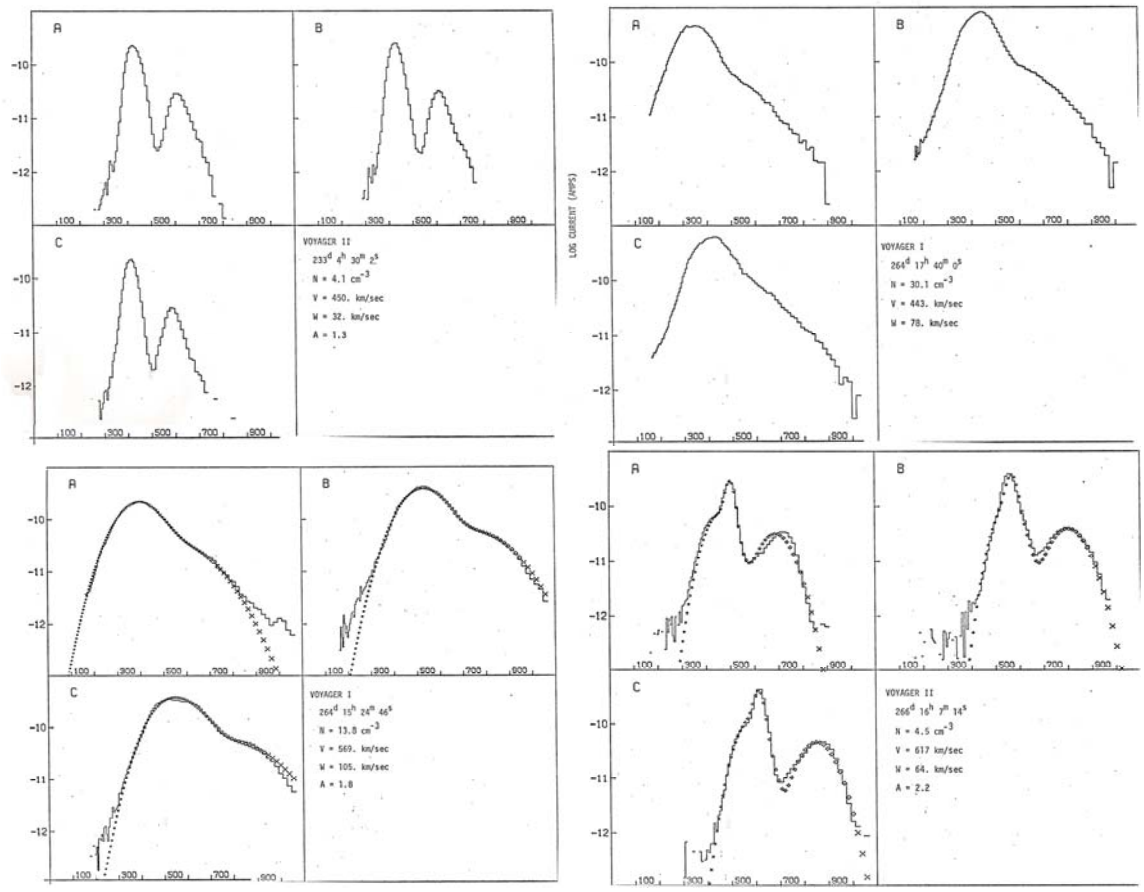

Figure 3.3-1: Examples of Measured Ion Currents in the M Mode

3.3.2 Heliosheath L Modes

Voyager 2 crossed the termination shock in August of 2007. Figure 3.3-2 shows a heliosheath spectra and least squares fit at the time indicated. Fit parameters are given at the bottom of the Figure.

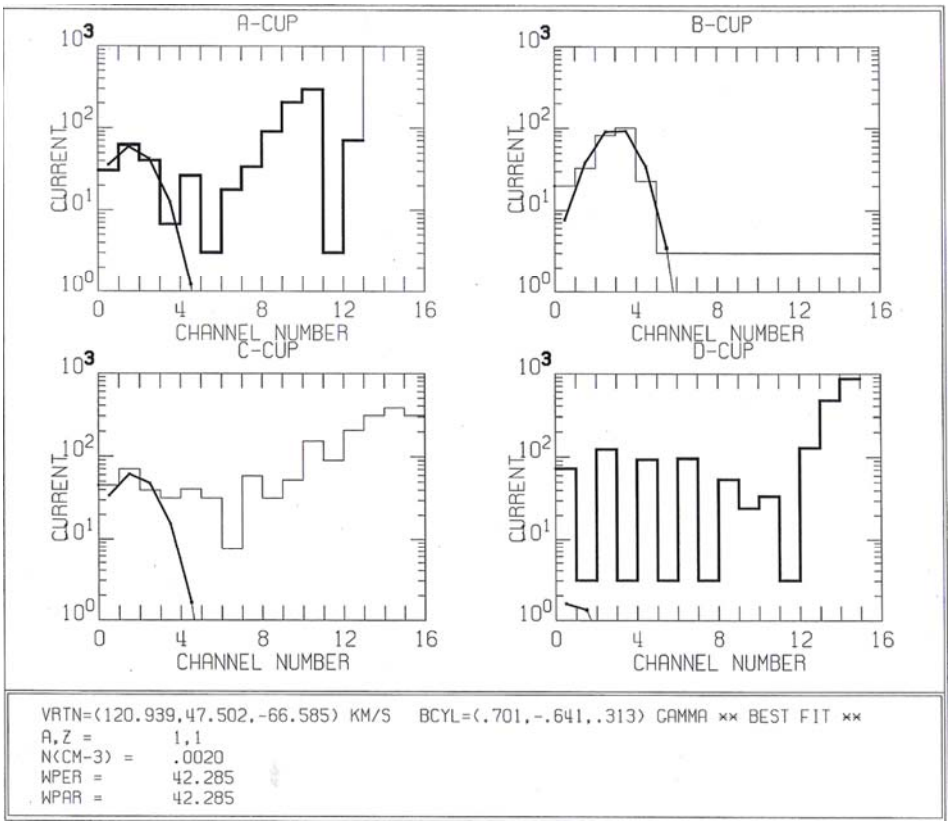

Figure 3.3-2: Heliosheath L Mode Spectra on 2007 day 267 1916 26.135

3.3.3 Fitting a Bi-Maxwellian to Voyager Spectra

In addition to the model independent moments calculation described above, we also frequently want to find a best fit of a bi-maxwellian to Voyager spectra. First we consider fitting a single maxwellian to one sensor. We assume the form of our reduced distribution function *F* is (see 3.2.2.4)

$$F(\mathrm{v}_n) = \int_{-\infty}^{\infty}\int_{-\infty}^{\infty} d\mathrm{v}_{t1} d\mathrm{v}_{t2}\, f\left(\mathrm{v}_n, \mathrm{v}_{t1}, \mathrm{v}_{t2}\right) = \frac{n}{\sqrt{\pi} w_n} e^{-(\mathrm{v}_n - V_n)^2 / w_n^2} \qquad (3.3.3.1)$$

This gives a density *n* of

$$n = \int_{-\infty}^{\infty} F(\mathrm{v}_n)\, d\mathrm{v}_n = \int_{-\infty}^{\infty} \frac{n}{\sqrt{\pi} w_n} e^{-(\mathrm{v}_n - V_n)^2 / w_n^2}\, d\mathrm{v}_n = \frac{n}{\sqrt{\pi}} \int_{-\infty}^{\infty} e^{-x^2}\, dx = n \qquad (3.3.3.2)$$

and a thermal speed w_n of (cf. 3.2.4.2)

$$w_n^2 = 2\int \left(\mathrm{v}_n - \mathrm{V}_n\right)^2 F(\mathrm{v}_n)\, d\mathrm{v}_n / n = 2\int \left(\mathrm{v}_n - \mathrm{V}_n\right)^2 \frac{n}{\sqrt{\pi} w_n} e^{-(\mathrm{v}_n - V_n)^2 / w_n^2}\, d\mathrm{v}_n \qquad (3.3.3.3)$$

$$w_n^2 = \frac{2}{w_n}\frac{n}{\sqrt{\pi}} w_n^3 \int x^2 e^{-x^2}\, dx = w_n^2 \tag{3.3.3.4}$$

If we now ask what the current in a given channel is when we integrate from the lower velocity window to the upper velocity window of the nth channel, it is given by (cf. 3.2.2.1)

$$I_k = q_{proton} A \int_{\mathrm{v}_k}^{\mathrm{v}_{k+1}} d\mathrm{v}_n \mathrm{v}_n \int_{-\infty}^{\infty}\int_{-\infty}^{\infty} d\mathrm{v}_{t1} d\mathrm{v}_{t2}\, f(\mathbf{v}) = qA_{eff} \int_{\mathrm{v}_k}^{\mathrm{v}_{k+1}} d\mathrm{v}_n \mathrm{v}_n F(\mathrm{v}_n) \tag{3.3.3.5}$$

$$I_k = qA_{eff} \int_{\mathrm{v}_k}^{\mathrm{v}_{k+1}} d\mathrm{v}_n \mathrm{v}_n \frac{n}{\sqrt{\pi} w_n} e^{-(\mathrm{v}_n - V_n)^2/w_n^2} = qA_{eff} \frac{n}{\sqrt{\pi} w_n} \int_{\mathrm{v}_k}^{\mathrm{v}_{k+1}} d\mathrm{v}_n \mathrm{v}_n e^{-(\mathrm{v}_n - V_n)^2/w_n^2} \tag{3.3.3.6}$$

The above function can be integrated but it involves the *erf* function. For most purposes we combine (3.2.2.5) with (3.3.3.1) to obtain

$$F(\mathrm{v}_n)\big|_{\mathrm{v}_n = \bar{\mathrm{v}}_k} = I_k \,/\left[q_{proton} A_{eff} \Delta \mathrm{v}_k \bar{\mathrm{v}}_k \right] = \frac{n}{\sqrt{\pi} w_n} e^{-(\mathrm{v}_k - V_n)^2/w_n^2} \tag{3.3.3.7}$$

and we use this to fit our measured currents to a maxwellian.

3.4 The Status Word

The status word is an 8 bit word that indicates the measurement mode of the instrument (*L* mode, *M* mode, low energy electron mode *E1*, and high energy electron mode *E2*), the gain of the instrument, and the calibration mode of the instrument. For example, a status word of 2F means that we are in the L mode and IGAN = 1 and ICAP = 0 and the instrument is taking plasma data with the modulator on.

3.4.1 Bits 1 and 2 of status word code L, E1, E2, M

Table 3.2 shows how the upper two bits of the status word encodes the measurement mode of the instrument.

Mode	Bits 1 and 2
L	(0,0)
E1	(0,1)
E2	(1,0)
M	(1,1)

Table 3-2: Bits 1 and 2 Code L, E1, E2, and M

3.4.2 Bits 3 and 4 of status word code IGAIN and ICAP

(IGAN,ICAP)	Bits 3 and 4
(0,0)	(0,0)
(0,1)	(0,1)
(1,0)	(1,0)
(1,1)	(1,1)

Table 3-3: Bits 3 and 4 Code IGAIN and ICAP

If IGAN = 0 the gain *G* is 2.0, if IGAN = 1 the gain *G* is 20.0; if ICAP = 0 the capacitance *C* is 0.15, and if ICAP = 1 the capacitance *C* is 1.15.

3.4.3 Bits 5 through 8 of status word code calibration modes

Calibration Mode	Bits 5-8	Hex Value	Integer Value
DC Return Modulator Off	(0,0,0,0)	0	0
Modulator Calibration	(0,1,1,1)	7	7
Internal Current Calibration	(1,0,1,0)	A	10
DC Return Modulator On	(1,1,0,1)	D	13
Plasma Data Modulator Off	(1,1,1,0)	E	14
Plasma Data Modulator On	(1,1,1,1)	F	15

Table 3-4: Bits 5-8 and Calibration Modes

3.4.4 Examples of Status Word Decoding

For the M mode on Voyager 2 taken at 1991 160 12 4 48 372, the status word LSTAT printed out in hex (Z) format is FFFF0000. The clock parameter JCLK is 3, meaning this data is taken at the 930 ms integration time. We only want to look at the first eight bits of LSTAT, which are (1,1,1,1,1,1,1,1). Bits 5-8 tell us that this is Plasma Data Modulator On (cf. Table 3-4). Bits 3 and 4 tell us that (IGAN,ICAP) is (1,1). Bits 1 and 2 tell us that we are in the M mode (cf Table 3-2). From Table 3-5 below, we thus see that the threshold current in femtoamps for DN to current conversion is 23.0 femtoamps.

For the L mode on Voyager 2 taken at 1991 160 12 0 54 132, the status word LSTAT printed out in hex (Z) format is 2F2F0000. The clock parameter JCLK is 3, meaning this data is taken at the 930 ms integration time. We only want to look at the first eight bits of LSTAT, which is (0,0,1,0,1,1,1,1). Bits 5-8 tell us that this is Plasma Data Modulator On. Bits 3 and 4 tell us that (IGAN,ICAP) is (1,0). Bits 1 and 2 tell us that we are in the L mode (0,0). From Table 3-5 below, we thus see that the threshold current in femtoamps for DN to current conversion is 3 femtoamps.

For the E1 mode on Voyager 2 taken at 1991 160 12 0 33 20, the status word LSTAT printed out in hex (Z) format is 6F6F0000. The clock parameter JCLK is 3, meaning this data is taken at the 930 ms integration time. We only want to look at the first eight bits of LSTAT, which is (0,1,1,0,1,1,1,1). Bits 5-8 tell us that this is Plasma Data Modulator on. Bits 3 and 4 tell us that (IGAN,ICAP) is (1,0). Bits 1 and 2 tell us that we are in the E1 mode (0,0).

For the E2 mode on Voyager 2 taken at 1991 160 12 1 15 260, the status word LSTAT printed out in hex (Z) format is AFAF0000. The clock parameter JCLK is 3, meaning this data is taken at the 930 ms integration time. We only want to look at the first eight bits of LSTAT, which is (1,0,1,0,1,1,1,1). Bits 5-8 tell us that this is Plasma Data Modulator On. Bits 3 and 4 tell us that (IGAN,ICAP) is (1,0). Bits 1 and 2 tell us that we are in the E2 mode (0,0).

The code in *ansprt.f* computes the following integers from the status word:

```
KSTAT = L1X(LSTAT)
IPLS = MOD(KSTAT/2,2)
ITYP = MOD(KSTAT/4,4)
```

The first of these commands takes the first eight bits of the status word LSTAT, so in the example above (LSTAT = 6F6F0000), it would (in hex format) be AF. In bit format this corresponds to (1,0,1,0,1,1,1,1). IPLS is this integer divided by 2 modulo two, which will isolate the second bit from the right in the above sequence, e.g. 1. ITYP is this integer divided by four, modulo 4, which will take the third and fourth bits from the right in the above above sequence. A comparison with Table 3-1 shows that normal plasma measurements should have IPLS = 1 and ITYP = 3. But this can either be mod on or mod off. To make sure we have the modulator on, compute the following.

```
IPLSON = MOD(KSTAT,16)
```

To make sure we are only looking at plasma data modulator on, take only values of IPLON of 15.

3.5 DN (digital numbers) and EU (engineering units)

3.5.1 Determining the Threshold

The threshold value T for a given gain G and capacitance C and integration time Δt is given by

$$T = 372.\frac{C}{G\Delta t} \qquad (3.5.1.1)$$

The values of C and G are determined from the status word and the integration time is specified independent of the status word on the EDR. Table 3-5 gives the range of threshold values possible.

Capacitance (ICAP)	Gain (IGAN)	Integration Time (JCLK)	Threshold
0.15 (0)	2 (0)	0.03 (1)	930
1.15 (1)	2 (0)	0.03 (1)	7130.00
0.15 (0)	20 (1)	0.03 (1)	93.00
1.15 (1)	20 (1)	0.03 (1)	713.00
0.15 (0)	2 (0)	0.21 (2)	132.86
1.15 (1)	2 (0)	0.21 (2)	1018.57
0.15 (0)	20 (1)	0.21 (2)	13.29
1.15 (1)	20 (1)	0.21 (2)	101.86
0.15 (0)	2 (0)	0.93 (3)	30.00
1.15 (1)	2 (0)	0.93 (3)	230.00
0.15 (0)	20 (1)	0.93 (3)	3.00
1.15 (1)	20 (1)	0.93 (3)	23.00

Table 3-5: Thresholds for Gains, Capacitances, and Integration Times

3.5.2 Formula for Conversion DN to EU

Given a DN value from 0 to 255, and the threshold current *T* calculated above, the EU is given by (in femtoamps)

$$EU = T * 10^{(DN/64)}$$

For 0 DN we recover the threshold of 3 femtoamps, and for a DN value of 255 we are at 10^4 times threshold. The dynamic range of the current measurements is thus four orders of magnitude.

3.6 Calibration Sequence in the Heliosheath

Table 3-6 shows the calibration sequence in the heliosheath.

# Frames	Status	Mode
2	3	
2	7	Mod Cal
2	A	Current Calibration
2	F	Plasma data Mod On
2	A	Current Calibration
2	D	DC Return Mod On
2	F	Plasma data Mod On
2	A	Current Calibration
2	F	Plasma data Mod On
2	A	Current Calibration
2	7	Mod Cal
2	F	Plasma data Mod On
2	A	Current Calibration
2	F	Plasma data Mod On
2	B	

Table 3-6: Calibration Sequence in the Heliosheath

4 Trajectory and Pointing

4.1 Coordinate Systems

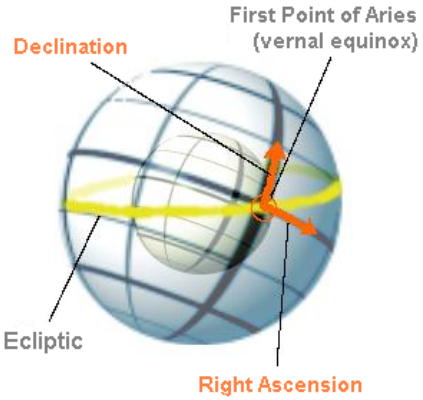

4.1.1 Earth Equatorial to Ecliptic ECL50

The right ascension α and declination δ of a star in earth equatorial coordinates can be used to compute the ECL50 XYZ components of the direction to the star as follows. First calculate the XYZ coordinates in earth equatorial coordinates using the following equation

$$\mathbf{X}_{\text{equatorial}} = \begin{pmatrix} \cos\delta\cos\alpha \\ \cos\delta\sin\alpha \\ \sin\delta \end{pmatrix} \tag{4.1.1}$$

Then rotate this vector about the X-axis by φ = 23.445789 degrees, the tilt of the earth's spin axis from the normal to the plane of its orbit, to get the coordinates of the vector in ECL50.

$$\mathbf{X}_{\text{ECL50}} = \begin{pmatrix} 1 & 0 & 0 \\ 0 & \cos\varphi & \sin\varphi \\ 0 & -\sin\varphi & \cos\varphi \end{pmatrix} \mathbf{X}_{\text{equatorial}} \tag{4.1.2}$$

4.1.2 ECL50

The ECL50 coordinate system is based on the ecliptic plane, that is, the plane of the orbit of the earth about the sun. The x-axis of this system is defined by the intersection of the plane of the earth's orbit with the plane of the earth's rotational equator, with zero longitude being defined in terms of the ascending node (see Figure 9.1-1).

4.1.3 RTN Heliographic

RTN Heliographic coordinates are based on the rotational equator of the sun (which defines the solar equatorial plane, see Figure 8.1-1). The normal to that plane is tilted at an angle of θ_s =7.25 degrees from the normal to the ecliptic. The intersection of the plane of the solar equator and of the ecliptic occurs defines the x axis of the RTN system, with the longitude of the ascending note (the x axis of RTN) at an angle of ϕ_s =75.07 degrees as measured in ECL50 coordinates.

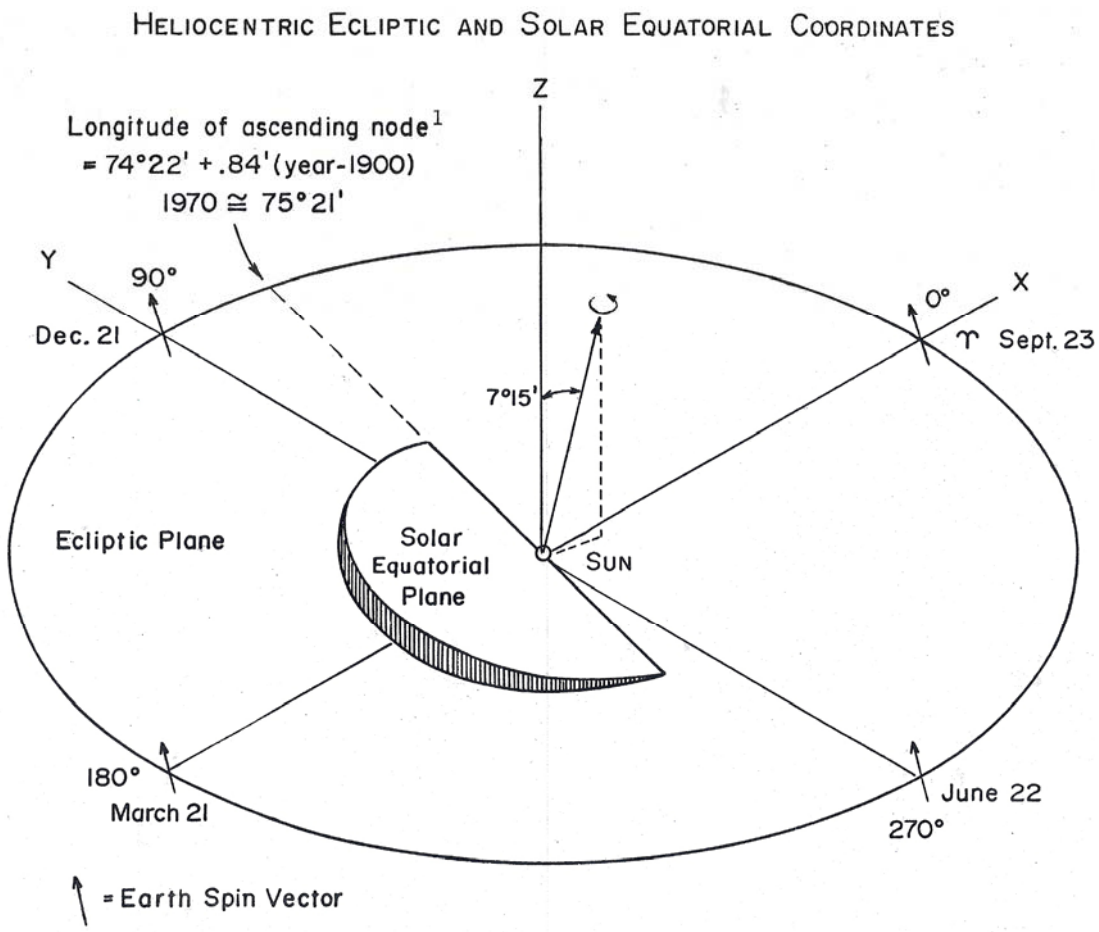

Figure 4.1: Ecliptic and Solar Equatorial Coordinates

To rotate from ECL50 to RTN coordinates, we first rotate in the *xy* ECL50 plane to get to the RTN x-axis and then rotate about the x-axis to tilt the z-axis over to the appropriate orientation. That is, if $\mathbf{X}_{ECL50}$ is a Cartesian coordinate vector in ECL50, then its Cartesian coordinate vector in RTN, $\mathbf{X}_{RTN}$, is given by

$$\mathbf{X}_{RTN} = \begin{pmatrix} 1 & 0 & 0 \\ 0 & \cos\theta_s & \sin\theta_s \\ 0 & -\sin\theta_s & \cos\theta_s \end{pmatrix} \begin{pmatrix} \cos\phi_s & \sin\phi_s & 0 \\ -\sin\phi_s & \cos\phi_s & 0 \\ 0 & 0 & 1 \end{pmatrix} \mathbf{X}_{ECL50} \tag{4.1.3}$$

or

$$\mathbf{X}_{RTN} = \begin{pmatrix} \cos\phi_s & \sin\phi_s & 0 \\ -\cos\theta_s \sin\phi_s & \cos\theta_s \cos\phi_s & \sin\theta_s \\ \sin\theta_s \sin\phi_s & -\sin\theta_s \cos\phi_s & \cos\theta_s \end{pmatrix} \mathbf{X}_{ECL50} \tag{4.1.4}$$

We can invert this easily to give

$$\mathbf{X_{ECL50}} = \begin{pmatrix} \cos\phi_s & -\sin\phi_s & 0 \\ \sin\phi_s & \cos\phi_s & 0 \\ 0 & 0 & 1 \end{pmatrix} \begin{pmatrix} 1 & 0 & 0 \\ 0 & \cos\theta_s & -\sin\theta_s \\ 0 & \sin\theta_s & \cos\theta_s \end{pmatrix} \mathbf{X_{RTN}} \tag{4.1.5}$$

or

$$\mathbf{X}_{RTN} = \begin{pmatrix} \cos\phi_s & -\cos\theta_s \sin\phi_s & \sin\theta_s \sin\phi_s \\ \sin\phi_s & \cos\theta_s \cos\phi_s & -\sin\theta_s \cos\phi_s \\ 0 & \sin\theta_s & \cos\theta_s \end{pmatrix} \mathbf{X}_{ECL50} \tag{4.1.6}$$

4.1.4 IHC Interstellar Heliospheric Coordinates

We now define IHC coordinates as a coordinate system whose z-axis lies in the direction opposite to the interstellar wind direction. This is the direction to the inflow of neutrals into the solar systems, and we use the directions given by Lallement et al. (1990). These authors give the direction to the incoming neutrals of ecliptic longitude λ of 252 degrees and ecliptic latitude β of 7 degrees, a speed of 20 km/s, and a temperature T of 8000 K. The components of this vector in ECL50 are

$$Z_{\mathrm{IHC}}^{\mathrm{ECL50}} = \begin{pmatrix} \cos\beta\cos\lambda \\ \cos\beta\sin\lambda \\ \sin\beta \end{pmatrix} = \begin{pmatrix} \text{-0.306714} \\ \text{-0.943967} \\ 0.121869 \end{pmatrix} \tag{4.1.7}$$

If we use the transformation from ECL50 to RTN given above this gives us

$$Z_{\mathrm{IHC}}^{\mathrm{RTN}} = \begin{pmatrix} \text{-0.991122} \\ 0.068112 \\ 0.1141867 \end{pmatrix} \tag{4.1.8}$$

Note that this vector lies almost in the solar equatorial plane.

Now we define the x-axis and y-axis of our IHC coordinates such that

$$\mathrm{X_{IHC}} = \frac{\mathbf{Z}_{\mathrm{RTN}} \times \mathbf{Z}_{\mathrm{IHC}}}{\left|\mathbf{Z}_{\mathrm{RTN}} \times \mathbf{Z}_{\mathrm{IHC}}\right|} \qquad \mathrm{Y_{IHC}} = \mathbf{Z}_{\mathrm{IHC}} \times \mathbf{X}_{\mathrm{IHC}} \tag{4.1.9}$$

which in RTN are given by

$$\mathrm{X}_{\mathrm{IHC}}^{\mathrm{RTN}} = \begin{pmatrix} -0.068560 \\ -0.997647 \\ 0.0 \end{pmatrix} \qquad \mathrm{Y}_{\mathrm{IHC}}^{\mathrm{RTN}} = \begin{pmatrix} 0.113918 \\ -0.007829 \\ 0.993459 \end{pmatrix} \tag{4.1.10}$$

Note that the z-axis in IHC is almost the negative x-axis in RTN, the x-axis in IHC is almost the negative y axis in RTN, and that the y-axis in IHC is almost the z-axis in RTN.

4.1.5 Ecliptic to Galactic Coordinates

We define GAC coordinates as a coordinate system whose z-axis lies in the direction of the north galactic pole, which is given in ecliptic coordinates $(\lambda_{GP}, \beta_{GP})$ by (180.01 degrees, 29.80 degrees). Thus in ECL50 we have

$$\mathbf{Z}_{\mathrm{GAC}}^{\mathrm{ECL50}} = \begin{pmatrix} \cos\beta_{GP} \cos\lambda_{GP} \\ \cos\beta_{GP} \sin\lambda_{GP} \\ \sin\beta_{GP} \end{pmatrix} = \begin{pmatrix} ? \\ ? \\ ? \end{pmatrix} \tag{4.1.11}$$

To construct our coordinate system we also use the direction to the center of the galaxy, which is given in ecliptic coordinates $(\lambda_{GC}, \beta_{GC})$ by (266.84 degrees,-5.54 degrees). Thus the direction to the center of the galaxy is given by

$$\mathbf{X}_{\text{To Galactic Center}}^{ECL50} = \begin{pmatrix} \cos\beta_{GC} \cos\lambda_{GC} \\ \cos\beta_{GC} \sin\lambda_{GC} \\ \sin\beta_{GC} \end{pmatrix} = \begin{pmatrix} ? \\ ? \\ ? \end{pmatrix} \tag{4.1.12}$$

Using these two vectors, we define the Y axis of our galactic coordinates as

$$\mathbf{Y}_{\mathrm{GAC}}^{\mathrm{ECL50}} = \frac{\mathbf{Z}_{\mathrm{GAC}}^{\mathrm{ECL50}} \times \mathbf{X}_{\text{To Galactic Center}}^{ECL50}}{\left| \mathbf{Z}_{\mathrm{GAC}}^{\mathrm{ECL50}} \times \mathbf{X}_{\text{To Galactic Center}}^{ECL50} \right|} = \begin{pmatrix} ? \\ ? \\ ? \end{pmatrix} \tag{4.1.13}$$

And the X axis then completes the right hand system.

$$\mathbf{X}_{\mathrm{GAC}}^{\mathrm{ECL50}} = \frac{\mathbf{Y}_{\mathrm{GAC}}^{\mathrm{ECL50}} \times \mathbf{Z}_{\mathrm{GAC}}^{ECL50}}{\left| \mathbf{Y}_{\mathrm{GAC}}^{\mathrm{ECL50}} \times \mathbf{Z}_{\mathrm{GAC}}^{ECL50} \right|} = \begin{pmatrix} ? \\ ? \\ ? \end{pmatrix} \tag{4.1.14}$$

4.1.6 Going from Measured Cup Speeds to Velocity in RTN or IHC

We summarize the procedure for going from a measurement of V_A, V_B, and V_C from the observed data to the velocity vector in RTN or IHC. First we use equations (2.2.11) through (2.2.13) to find the velocity components in s/c coordinates. Then we use the pointing information from the SEDR (see Section 8.5 below), which gives the s/c axes in ECL50, to find the velocity components in ECL50. Then we must correct for aberration by ***adding*** the s/c velocity in ECL50 coordinates to the velocity vector in ECL50 we just computed. The s/c velocity in ECL50 is also given in the SEDR. Then we have the velocity vector in ECL50, and we can transform that vector from ECL50 to RTN or IHC using the transformations given above.

4.2 Lock stars

We show below a table that gives the common lock stars for Voyager, their right ascension and declination, and their ECL50 coordinates, computed using equations 8.1.1 and 8.1.2.

Table 4-7: Lock stars and their ECL50 Coordinates

Lock Star	Declination α	Right Ascension δ	X ECL50	Y ECL50	Z ECL50
CANOPUS	-52.6674	95.7107	-0.060344	0.237243	-0.969574
RIGILKENTAURUS	-60.6243	218.9856	-0.381294	-0.629850	-0.676686
HADAR	-60.133	210.0684	-0.430973	-0.573945	-0.696311
ACRUX	-62.8222	185.9498	-0.454293	-0.397389	-0.797308
SPICA	-10.9012	200.6384	-0.918936	-0.392778	-0.035792
ARCTURUS	19.4253	213.3351	-0.787912	-0.343138	0.511322
MIMOSA	-59.4158	191.1954	-0.499122	-0.433160	-0.750500
MIAPLACIDUS	-69.5101	138.1616	-0.260792	-0.158497	-0.952295
VEGA	38.74	278.81	0.119463	-0.458163	0.880804
FOMALHAUT	-29.89	343.73	0.832263	-0.421122	-0.360548
ALKAID	49.5621	206.3913	-0.581023	0.038322	0.812984
ACHERNAR	-57.4905	23.9654	0.491107	-0.135258	-0.860534
DENEB[1]	45.27	310.325	0.45542	-0.20958	0.86526

4.3 Generating Pointing Given the Lockstar and $\mathbf{Z}_{s/c}$

If we know the vector $\mathbf{Z}_{s/c}$ and the lockstar, we can compute the orientation of the spacecraft axes as follows. Let **S** be the vector in ECL50 of the lockstar, and assume we

[1] From http://www.astro.utoronto.ca/~garrison/oh.html

know the spacecraft z-axis in ECL50 as well (this is the earth spacecraft vector, and is usually given in the navigation block of the SEDR). We define the two directions

$$\hat{\mathbf{Y}}_S = \frac{\hat{\mathbf{Z}}_{s/c} \times \mathbf{S}}{\left|\hat{\mathbf{Z}}_{s/c} \times \mathbf{S}\right|} \qquad \hat{\mathbf{X}}_S = \hat{\mathbf{Y}}_S \times \hat{\mathbf{Z}}_{s/c} \tag{4.3.1}$$

Given this construction, we can compute the spacecraft **X** and **Y** axes using the equations (refer to Figure 2.2-1 and Section 2.3)

$$\hat{\mathbf{X}}_{s/c} = \hat{\mathbf{X}}_S \cos 55^o + \hat{\mathbf{Y}}_S \sin 55^o \tag{4.3.2}$$

$$\hat{\mathbf{Y}}_{s/c} = \hat{\mathbf{Y}}_S \cos 55^o - \hat{\mathbf{X}}_S \sin 55^o \tag{4.3.3}$$

For example, on the Short SEDR file for $2009^y\ 1^d\ 23^h\ 59^m\ 59s\ 1^{ms}$, the vector for the spacecraft z-axis in ECL50 is given as (0.2663, -0.8042, 0.5313). If we assume the lock star is Vega and use its ECL50 components as given in Table 8.1, then we find using the equations above that the predicted spacecraft X axes has ECL50 components of (-0.7024,-0.5394,0.4644) and the predicted spacecraft Y axis has components of (-0.6601,0.2495,-0.7086). These are the same as the values given in the pointing block to four significant figures.

$$\hat{\mathbf{n}}_A = -\hat{\mathbf{X}}_{s/c} \sin 20^o \cos 30^o - \hat{\mathbf{Y}}_{s/c} \sin 20^o \cos 60^o - \hat{\mathbf{Z}}_{s/c} \cos 20^o \tag{4.3.4}$$

5 Appendices

5.1 Voyager Memo #187: Optimal Lock Star Heliosheath and Interstellar Flow

To: Voyager Internal, E. J. Franzgrote, O. Divers
From: John Belcher
Subject: Optimal Lock Star for Detecting Heliosheath and Interstellar Flow
Date**:** March 1, 1994

The purpose of this memo is to determine the optimal lock star for PLS for observations while the spacecraft is in the heliosheath or in the interstellar medium (e.g., post termination shock or post heliopause). We conclude that of the available lock stars for Voyager 2 with Canopus ratio (CR) greater than 0.25, Vega is the optimal lock star for PLS. This conclusion is based on the list of available lock stars given in the table on page JCH-3 of the minutes for the SSG meeting of 4/21/92. Deneb is the preferred lock star for PLS of the lock stars in this table, but its CR is only 0.18. If that precludes its use as a lock star, then PLS prefers Vega for the lock star.

To justify this conclusion, we make the plausible assumption that the plane containing heliosheath and interstellar flow is the plane defined by the sun-spacecraft

vector and the interstellar neutral wind vector, as defined by Lyman alpha measurements. To optimize the ability to measure heliosheath and interstellar plasma, we need to orient the PLS side sensor (the D cup) so that its normal lies as close as possible to being in the plane expected for such flow, with this flow having a positive component into the D cup.

For reference, the figure below shows the trajectory of the Voyager 2 spacecraft in a cylindrical sun-centered coordinate system where the horizontal axis is along the direction from which the interstellar wind flow comes and the vertical axis is cylindrical distance from this axis. We also show on this Figure model heliopause and termination shock shapes.

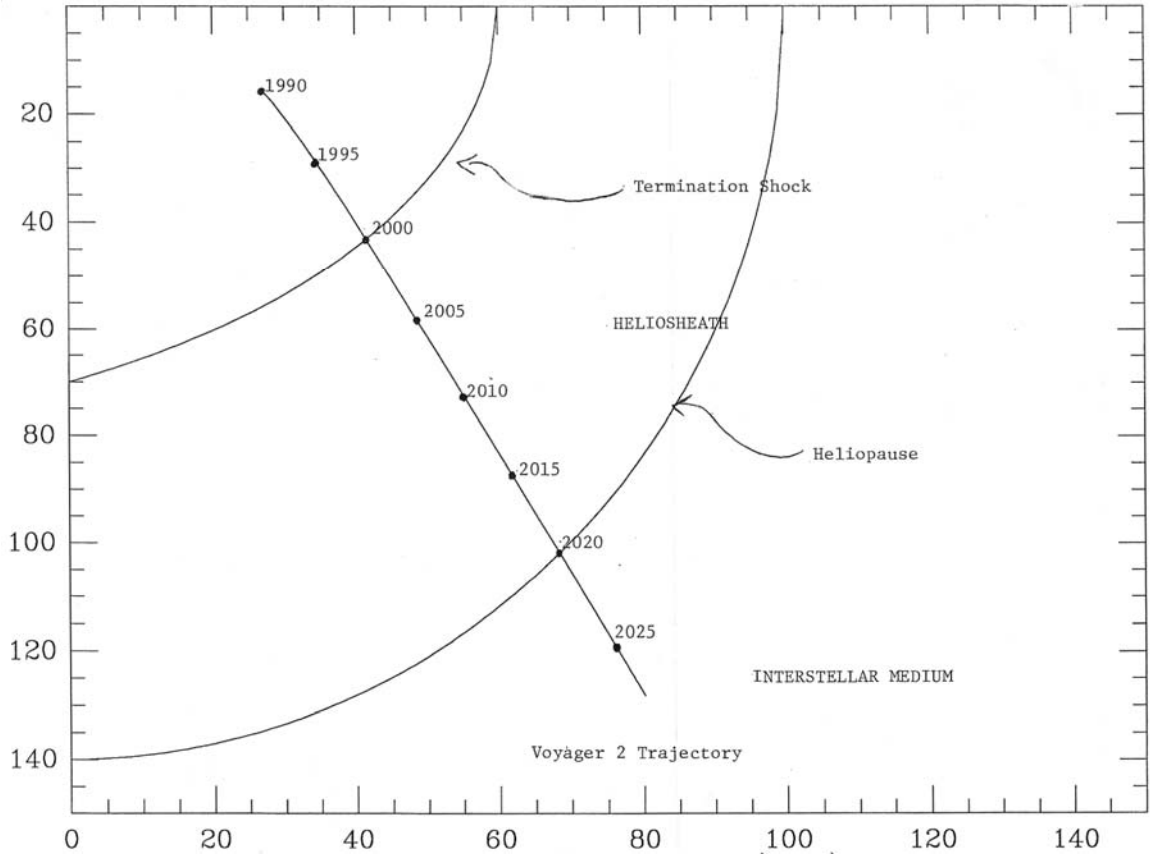

Figure 5.1-1: Trajectory of Voyager 2

The figure below shows the optimal roll angle of the spacecraft with respect to Canopus for detecting heliosheath and interstellar flows, as a function of time from 1995 through 2030. This is the roll angle that puts the D cup normal in the plane containing such flow, as defined above. The last section of this memo gives ECL50 components of various vectors of interest, for reference purposes. The roll angle of Vega (the current planned lock star in this epoch) with respect to Canopus is about 180 degrees. The roll angle of Spica (the lock star requested by LECP) with respect to Canopus is about -90 degrees. The roll angle of Arcturus with respect to Canopus is about -120 degrees. The roll angle of Deneb with respect to Canopus is about 158 degrees. Vega, Spica, and

Arcturus are the three lock stars with CR's greater than 0.25. Of these three, Vega is clearly preferred. Deneb is better than Vega, but has a CR less than 0.25.

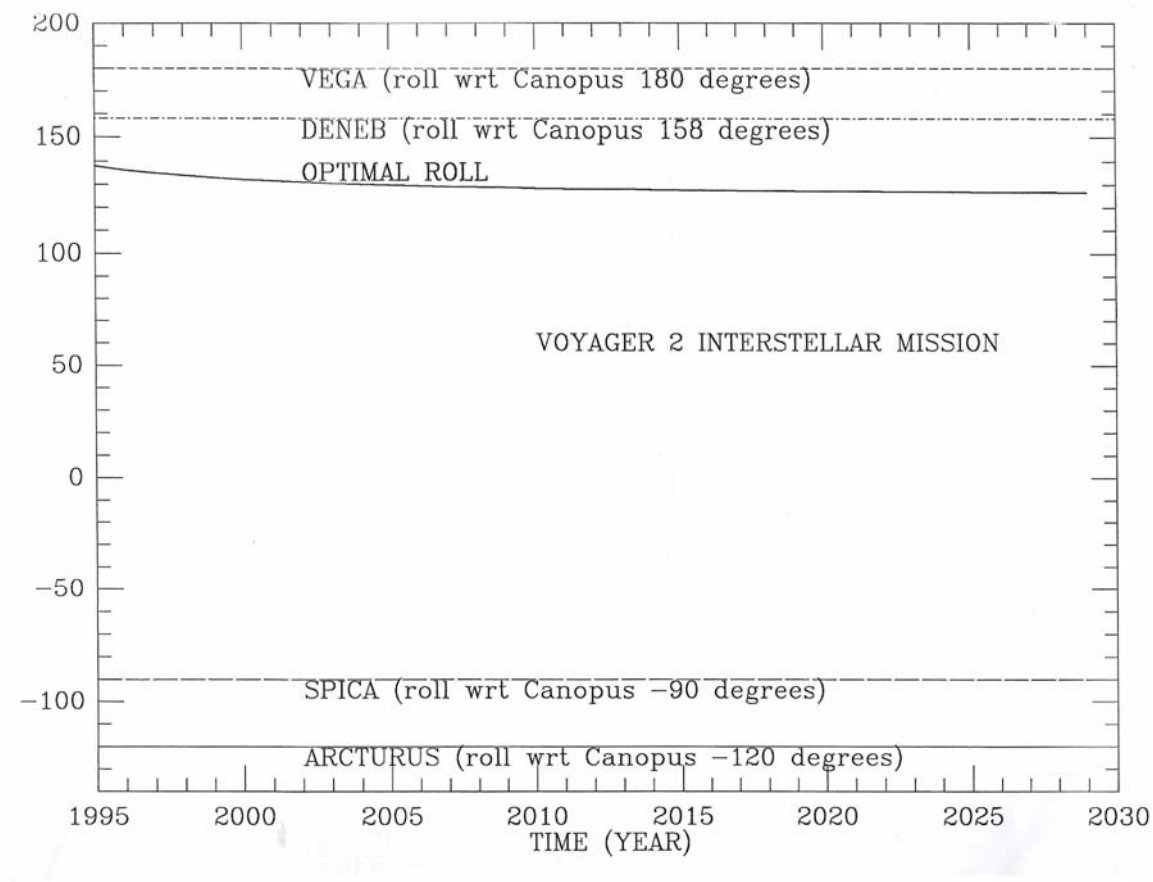

Figure 5.1-2: Optimal role with respect to Canopus versus time

Model Heliosheath and Interstellar Flows

To understand more clearly why Vega and Deneb are preferred over Spica and Arcturus, the next two figures below show characteristics of the flow of heliosheath and interstellar ions into the PLS sensors as a function of time, for the four different lock stars. These figures have been produced using the following scenario for crossing of the termination shock and heliopause:

1. From 1995 until 2000, Voyager 2 is in the unshocked solar wind, and the plasma flow is solar wind flow at 400 km/s radially away from the sun.
2. In 2000, Voyager crosses the termination shock. For the next 20 years, until 2020, Voyager 2 is in the heliosheath. In this period, we assume that the shocked solar wind has a speed of 200 km/s. We assume that the flow direction in 2000, and that just after the shock crossing, is still radially away from the sun. Over the course of the next 20 years, the flow direction turns from radially away from the

sun toward the direction of the interstellar wind. That is, the flow direction varies linearly with time over this interval, until it is within 30 degrees of being along the direction of the interstellar wind, in 2020.

3. In 2020, Voyager 2 crosses the heliopause. It is then in the shocked interstellar medium. We assume that the flow speed there is 20 km/s, the speed derived for interstellar neutrals from Lyman alpha measurements. For the flow direction, we assume that the flow is 30 degrees from the interstellar wind direction, deflected toward the radial direction. This would be appropriate for flow deflected by the solar cavity along the flanks of the heliosphere. For all these cases, the plasma flow is properly aberrated for spacecraft velocity.

The figure below shows as a function of time the angle that this model flow makes with the normal to the A cup, for the four different lock stars we have mentioned. The A cup is the cup in the main sensor cluster whose normal is furtherest away from the D cup normal.

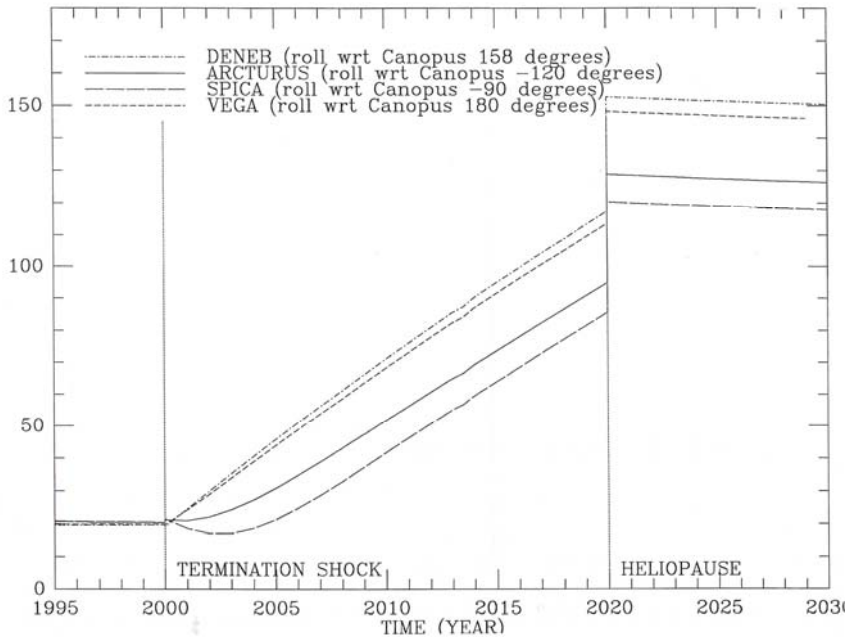

Figure 5.1-3: Angle between A sensor normal and heliosheath flow direction

The figure below is similar to the figure above, except we consider the D cup in this Figure. Before the terminal shock, the flow is 20 degrees from being directly into the A cup (0 degrees is into the cup). After the terminal shock is crossed, the flow makes a greater and greater angle to the A cup normal, as it turns from radial towards the direction of the interstellar wind. Eventually, the flow begins to come from the back of the A cup (the angle is greater than 90 degrees). For the D cup, in contrast, the flow starts out essentially perpendicular to the D cup normal before the terminal shock is crossed, for all four lock stars. After the shock, the flow turns so that it is closer to being into the D cup (the angle decreases) for Vega and Deneb. In contrast, the flow turns so that it is further away being into the D cup for Arcturus and Spica. Having the D cup in the Vega or Deneb orientation is crucial to being able to determine flow directions as the heliosheath flow turns toward the interstellar wind direction. At some point, having the D cup in this

orientation may be crucial to detecting the flow at all, since in the later years, before the heliopause crossing, the flow may be coming from the back of the main sensor cluster.

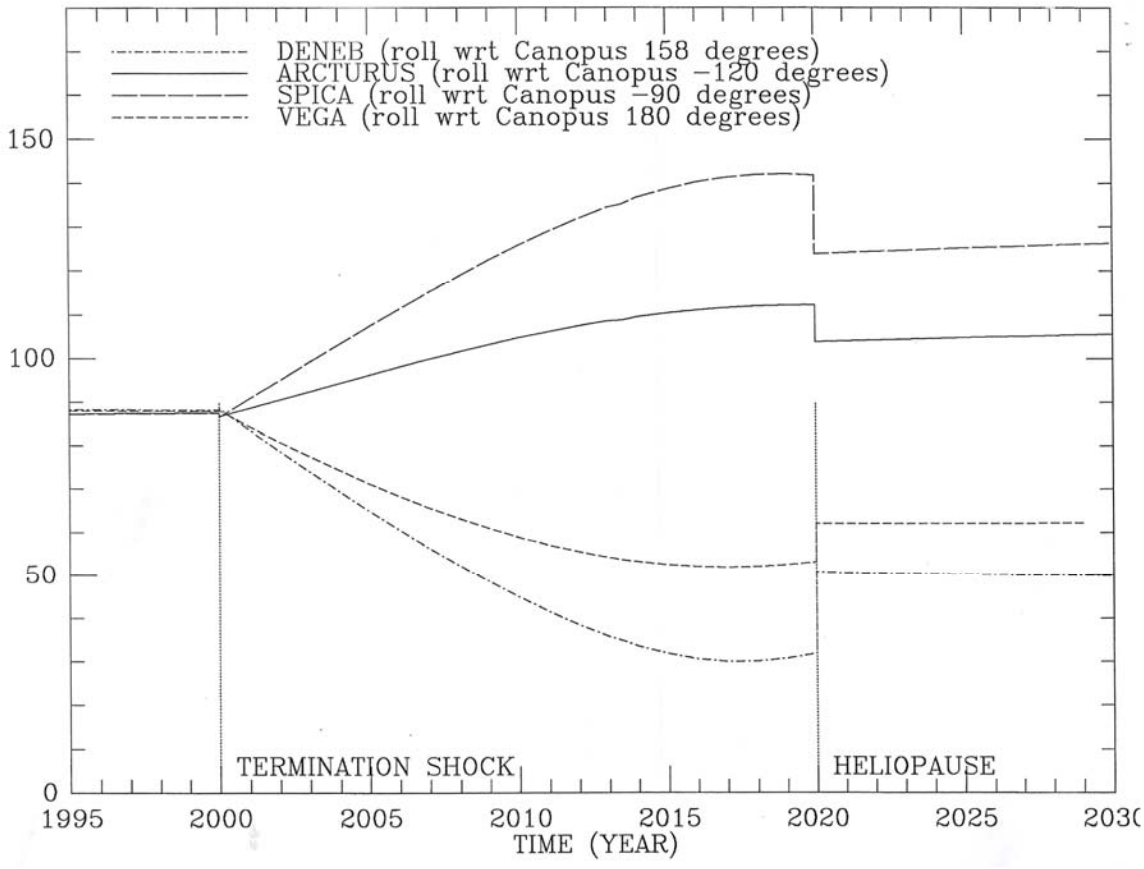

Figure 5.1-4: Angle between D sensor normal and heliosheath flow direction

When the heliopause is crossed, there is an abrupt change in apparent flow angle into both the A and the D cups, even though there is no change in the direction of the direction of the flow in an inertial sun-centered system. This change occurs because of the larger effects of aberration due to spacecraft velocity, as the model speed drops from the 200 km/s we have assumed to be characteristic of heliosheath flow, to the 20 km/s we have assumed for the shocked interstellar flow.

The reasons for the behavior of the angles shown in the figures above can be easily understood by considering the geometry, as illustrated in the figure below. The plane of this figure contains the sun-spacecraft line and the interstellar wind direction in 2010. Assuming the spacecraft is at a roll angle of 180 degrees (Vega),we show the projection of the D cup and the A cup normals onto this plane, and the projection of the spacecraft velocity onto this plane. The A cup normal makes an angle of 17 degrees with respect to this plane, and the D cup normal makes an angle of 67 degrees with respect to this plane. The spacecraft velocity is within 10 degrees of being in the plane. The magnitude of the spacecraft speed is 15.5 km/s at this time. Although we show these vectors in 2010, there is little qualitative change in the geometry past 2000.

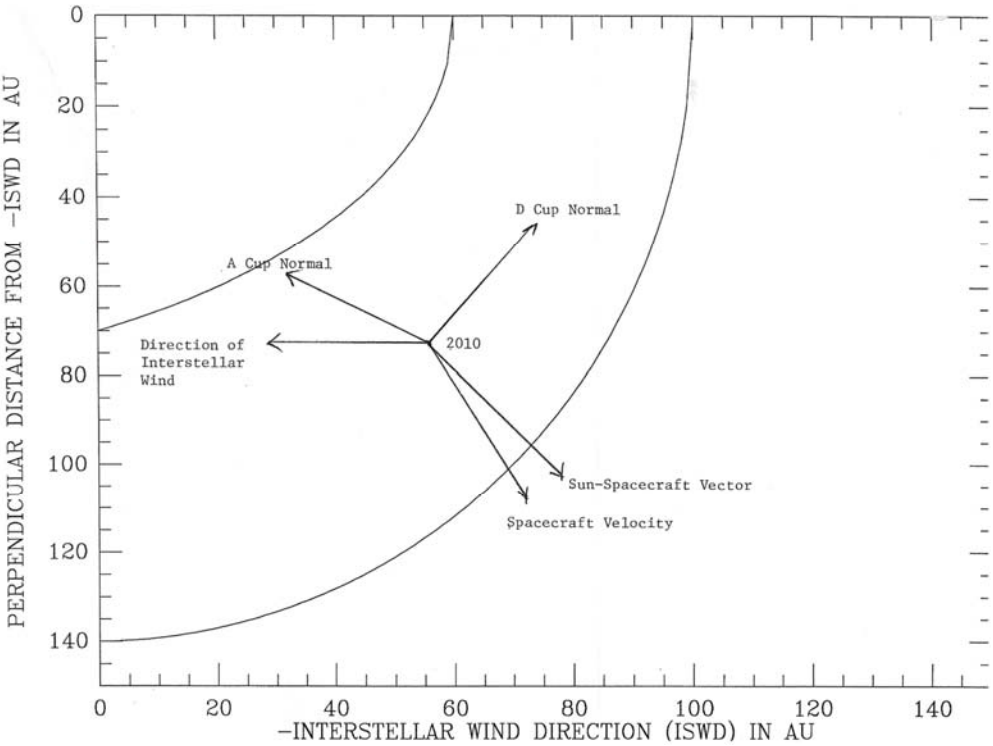

Figure 5.1-5: PLS A and D Cup Normal Orientation in 2010

In consideration of the figure above, it is clear that when the flow is radially away from the sun in our model, it is more or less into the A cup. After 2000, as the flow changes from radially away from the sun towards the interstellar wind direction, the flow moves out of the A cup and increasingly into the D cup, when the lock star is either Vega or Deneb. This explains the qualitative behaviors we discussed above.

As far as flows in the heliosheath are concerned, it is clear from these figures that Deneb is the preferred lock star, with Vega second. If Deneb cannot be used because of its CR, then Vega is the preferred lock star.

Simulation of Interstellar Proton Observations

It is also interesting to note that in the (relatively unlikely)event that Voyager 2 crosses the heliopause in its lifetime, there is some chance that the PLS instrument will be able to detect interstellar protons. We show in the next figure a model calculation of observations in the D cup of interstellar protons moving at the velocity of our model in the post heliopause region (a speed of 20 km/s at a deflection angle of 30 degrees from the direction of the interstellar neutral flow, with appropriate aberration).We assume a thermal speed of 20 km/s and a density of 1 proton per cubic centimeter. The Figure shows the expected currents in the M-mode, for the lock star Vega. On this lock star, the current in the first channel in the M-mode D cup is about 180 femtoamps. This current will scale as the density for other densities than our assumed one.

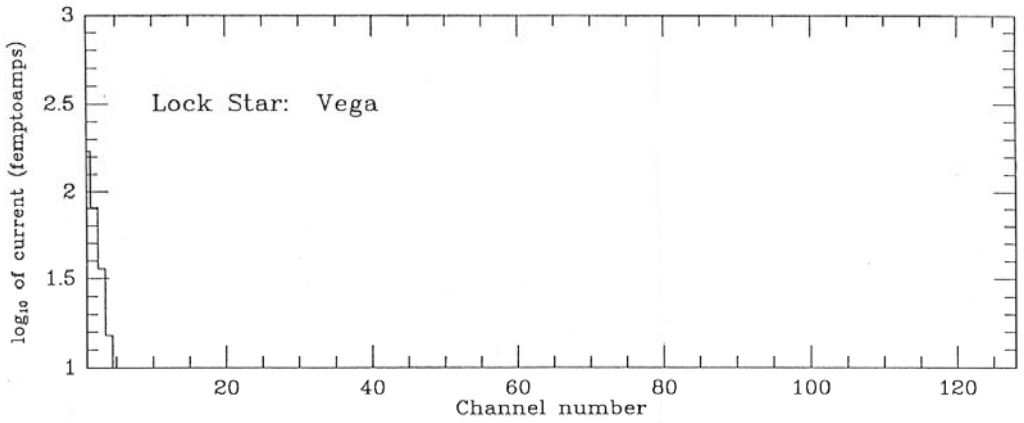

Figure 5.1-6: Model calculation of observations in the D cup of interstellar protons

The next figure shows the lower channels of the M-mode from a recent Voyager 2 observation of the solar wind. Our threshold in this mode is around 3 femtoamps, with a noise level of the order of 30 femtoamps. Thus we in principle may be able to detect interstellar ions with densities of the order of 30 femtoamps/180 femtoamps times 1 per cubic centimeter, or around 0.2 protons per cubic centimeter, and perhaps considerably less than this using long term averaging of many M-modes. Assuming local thermodynamic equilibrium, interstellar protons are thought to have densities on the order of 0.01 per cubic centimeter and less, but there are no direct measurements (seeW. I. Axford, "The Heliosphere", in Physics of the Outer Heliosphere, edited by S. Grzedzielske and D. E. Page, Cospar Colloquia Series, Pergamon Press, 1990). There is some chance that PLS may be able to detect interstellar ions directly, although clearly this is on the edge of what is possible.

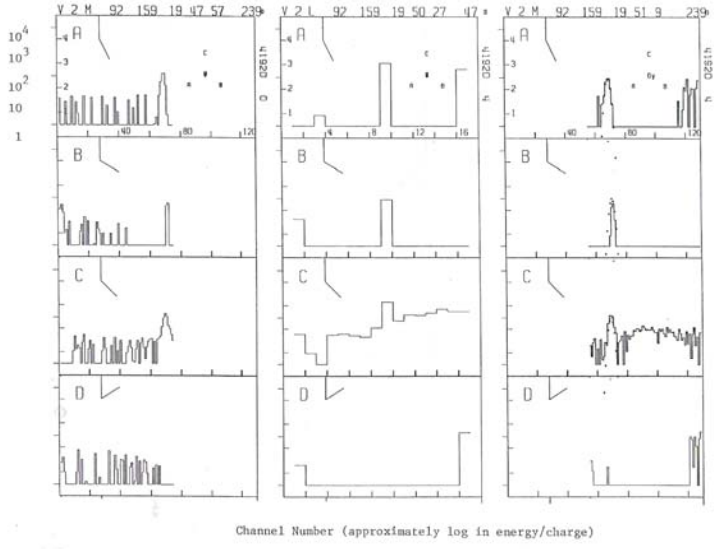

Figure 5.1-5: Voyager 2 observations in 1992

Interstellar Wind Direction

We use the direction of the interstellar wind as quoted by R. Lallement, J. L. Bertaux, E. Chassefiere, and B. R. Sandelin "Lyman-Alpha observations from Voyager (1-18 AU)", in the book cited above, page 74 (but also see below). They give the direction to the incoming neutrals of ecliptic longitude λ of 252 degrees and ecliptic latitude β of 7 degrees, a speed of 20 km/s, and a temperature T of 8000 K. This leads to a unit direction of the interstellar wind (which points opposite the incoming direction) in ECL50 Cartesian coordinates of (0.307,0.944,-0.122). In 2000, the unit vector from the sun to the spacecraft in ECL50 Cartesian coordinates is (0.254,-0.871,-0.421). The cross product of this vector with the interstellar wind vector, normalized so that it is a unit vector, is (0.699,-0.136,0.702). This is the normal to the plane containing the heliosheath flow in the year 2000.

Updated wind direction: The article by Lallement et al. Science **307** 1447 (2005) gives the angles as ecliptic longitude λ 252.2 degrees and ecliptic latitude β of 9 degrees.

Index